Research Article | Vol. 9, No. 9 | 1 Sep 2018 | BIOMEDICAL OPTICS EXPRESS 4263
Biomedical Optics EXPRESS

Miniature scanning light-sheet illumination implemented in a conventional microscope

ANJAN BHAT KASHEKODI, TOBIAS MEINERT, REBECCA MICHIELS, AND ALEXANDER ROHRBACH*

Laboratory for Bio-and Nano Photonics, Department of Microsystems Engineering - IMTEK, University of Freiburg, Freiburg 79110, Germany
**rohrbach@imtek.de*

Abstract: Living cells are highly dynamic systems responding to a large variety of biochemical and mechanical stimuli over minutes, which are well controlled by e.g. optical tweezers. However, live cell investigation through fluorescence microscopy is usually limited not only by the spatial and temporal imaging resolution but also by fluorophore bleaching. Therefore, we designed a miniature light-sheet illumination system that is implemented in a conventional inverted microscope equipped with optical tweezers and interferometric tracking to capture 3D images of living macrophages at reduced bleaching. The horizontal light-sheet is generated with a 0.12 mm small cantilevered mirror placed at 45° to the detection axis. The objective launched illumination beam is reflected by the micro-mirror and illuminates the sample perpendicular to the detection axis. Lateral and axial scanning of both Gaussian and Bessel beams, together with an electrically tunable lens for fast focusing, enables rapid 3D image capture without moving the sample or the objective lens. Using scanned Bessel beams and line-confocal detection, an average axial resolution of 0.8 µm together with a 10-15 fold improved image contrast is achieved.

1. Introduction

The detailed investigation of living cells represents one of the biggest challenges in optics, since cellular structures scale down to molecular dimensions with dynamics on millisecond timescales [1]. In addition, all live-cell studies based on fluorescence microscopy are limited by the lifetime of the fluorophores and their excited states. Fluorophores are destroyed after about 10^5 – 10^6 excitations, leading to exponential blackout (bleaching) and hence to the end of the imaging experiment. In addition, the fluorophores' excited state lifetime of some nanoseconds limit the number of emitted photons per time and therefore restricts the signal-to-noise ratio in the image at short integration times. A minimal integration time, on the other side, is necessary to achieve maximal temporal resolution in live cell imaging [2].

Light-sheet microscopy (LSM) [3, 4] is known to reduce photobleaching significantly [5], since only fluorophores in the focal plane are excited, but not those off-axis contributing to unnecessary background signals. In addition, LSM scans 3D objects plane-wise [3, 6] or line-wise [7, 8] and is therefore significantly faster than point-scanning microscopy.

Several schemes of light-sheet illumination are implemented apart from selective plane illumination microscopy (SPIM) to meet the specific requirements of different scientific communities. The published schemes include highly inclined laminated optical sheet (HILO) [9], inverted selective plane illumination microscopy (iSPIM) [10], reflected light-sheet microscopy (RLSM) [11], prism-coupled light-sheet Bayesian microscopy (LSBM) [12], single objective selective plane illumination microscopy (soSPIM) [13], swept confocally-aligned planar excitation (SCAPE) microscopy [14] and oblique plane microscopy (OPM) [15]. Bruns et al. developed an add-on light-sheet module for inverted microscopes [16].

Light-sheet microscopy has also been combined with optical tweezers to mount the whole sample by optical forces [17] or to probe the mechanical properties of epithelial cell junctions in embryos [18]. However, most of these schemes are significantly different to conventional

#340134 https://doi.org/10.1364/BOE.9.004263
Journal © 2018 Received 25 Jul 2018; accepted 2 Aug 2018; published 14 Aug 2018

Biomedical Optics EXPRESS

inverted microscopes, which are best suitable for advanced optical trapping and tracking such as in Photonic Force Microscopy (PFM). In PFM, directed and thermal motions of particles trapped nearby living cells are measured interferometrically at MHz rates in 3D [19–21].

In this study, we present a miniatured scheme of scanning light-sheet illumination, which is suitable for most inverted microscopes, even for the frequent case that an opposing objective lens confines the upper space significantly.

1.1 The setup scheme

Our microscope has two high NA objectives (Zeiss C-Apochromat 63x/1.20W and Zeiss W Plan-Apochromat 63x/1.0) opposite to each other, separated by a distance of less than 2 mm. Cells are placed on the coverslip inside the sample holder either in aqueous solution or transparent gels as shown in Fig. 1(a). A highly focused laser beam (NIR at 1064 nm, half-focus angle $\alpha \approx 60°$) is formed by the trapping objective lens leading to a stable 3D optical trap for beads with 0.5-3 µm in diameter. The NIR-tracking objective from above collects the unscattered light and light scattered at the beads, enabling precise and fast back focal plane (BFP) position tracking of the bead [22, 23]. The sample is not accessible from the side due to the confined geometry of the PFM setup (Fig. 1(a)). Hence, conventional methods to generate a light-sheet inside the sample using an additional horizontal illumination lens were unworkable in this configuration. Therefore, we designed a scheme where the trapping objective lens is used for both light-sheet illumination and fluorescence imaging. The slightly focused, horizontal beam, which is scanned laterally to form the light-sheet, is generated after the reflection from a small mirror placed at an angle of 45° to the detection axis using a cantilever holder. As shown in Fig. 1(b), a narrow illumination beam with an offset from the optical axis is deflected by the mirror and illuminates the sample perpendicular to the detection axis. 2D images were illuminated with horizontal scanning, while a 3D image stacks is obtained by vertical beam displacement and refocusing on the camera by an electro-optical tunable lens.

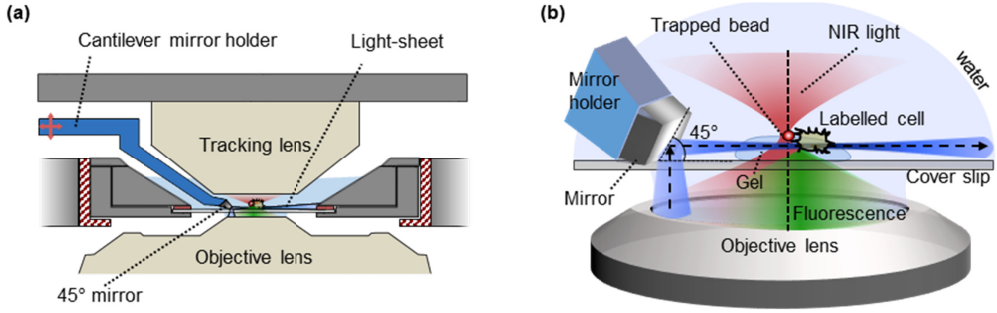

Fig. 1. Scheme for light-sheet generation inside the sample above the coverslip. (a) A small mirror is positioned at 45° to the detection axis using a precision cantilever holder. A narrow illumination beam, deflected by the mirror, illuminates the sample perpendicular to the detection axis. (b) The design of the mirror and the holder enables 3D imaging simultaneous to optical trapping and tracking.

1.2 The optical configuration

The optical components of the illumination and detection path are shown in Fig. 2. The illumination path can accommodate both Gaussian and Bessel illumination with minimal changes. The illumination laser beam at 491 nm (Cobolt Calypso 25mW) is 2x expanded before illuminating the center of an NA = 0.3 glass axicon. The Bessel beam generated behind the axicon is transferred by the lens pair (L1 and L2) to the front of the scan mirror (SM, Newport FSM-300). For Gaussian beam generation, the axicon is replaced with a lens of focal length 100 mm, which results in narrow beam with lower NA. The distance between lens L2 and the scan mirror is slightly longer than the focal length of lens L2 (f = 100 mm).

Biomedical Optics EXPRESS

This results in a diverging beam at the scan mirror and a diverging beam at the conjugate back focal plane inside the objective lens (OL). Hence, the focal plane of the illumination is forward shifted and 90° rotated from P3 to P4 through the 45° mirror. Consequently, plane P1 is conjugate to the focal plane P3 and the shifted image plane P2 conjugate to plane P4. The distance between L2 and SM was calculated by ray transfer matrix analysis and depends on the beam offset distance z_{off} ≈200 µm (see inset of Fig. 2). This distance can be fine-tuned to align the illumination beam center (as the thinnest part of the light-sheet) to the center of the sample or to the center of the detection optical axis.

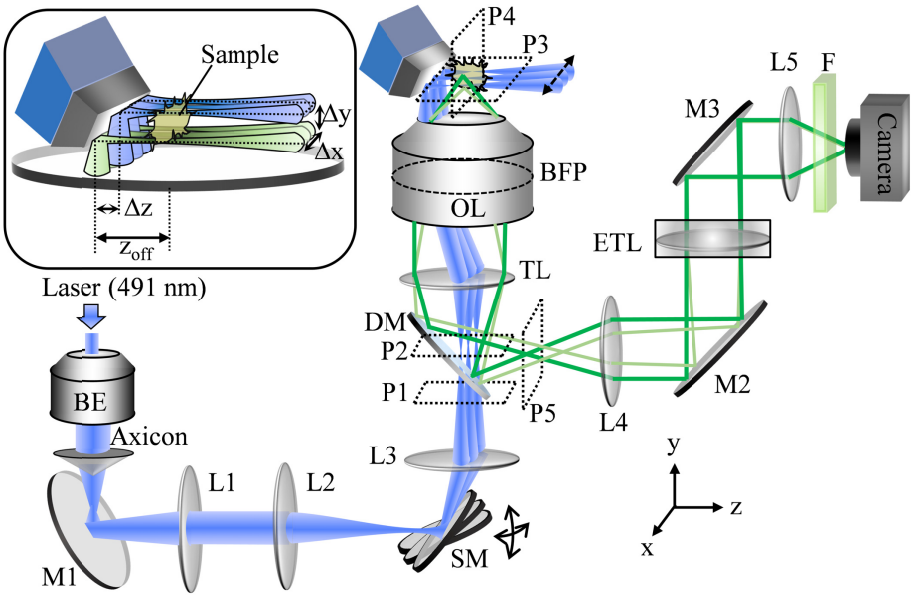

Fig. 2. Optics scheme of light-sheet generation and scanning. A laser beam is expanded (BE) and hits an axicon (NA = 0.3). Lenses L1 (f = 50 mm) and L2 (f = 100 mm) form a Bessel beam in front of the scan mirror (SM). The distance between lens L2 and the scan mirror is around 120 mm for a horizontal beam shift z_{off} ≈200 µm. The lens L3 and the tube lens (TL) conjugate the SM on to the back focal plane (BFP) of the objective lens (OL). The scan mirror tilts the beam at the BFP, such that the illumination beam is shifted at the sample plane. The 45° micro mirror placed at this position reflects the beam perpendicular to the detection. Beam scanning in x-direction results in light-sheet illumination of a 2D sample plane. The inset figure shows how different planes of the sample are illuminated by tilting the scan mirror in z-direction. The 45° mirror translates Δz to Δy, thus enabling the scanning in vertical y-direction. Planes P1 and P5 are conjugate to the sample plane P3. Plane P2 is conjugate to P4, the thinnest part of the light-sheet. On the detection side, the electrically tunable lens (ETL) at the conjugated BFP controls the refocusing of the objective. The dark and light green lines represent 2 different optical paths/planes, which are focused by the ETL onto the camera. The refocusing of the ETL is synchronized with the beam scanning in y-direction to acquire 3D image stacks

The detection path consists of an electrically tunable lens (ETL, Optotune EL-10-30-C-VIS-LD-MV), which is placed in a plane conjugate to the BFP of the OL, and is located between the relay lenses L4 and L5. The intermediate image plane P5 is conjugate to the sample plane P3. Lenses L4, ETL and L5 transfer the image to the camera. A narrow band fluorescence filter (F) blocks the reflected laser light. The focal power of the ETL determines the sample plane, which is imaged onto the camera. This technique was used to capture a complete 3D image of the sample without moving the objective or the sample, which enables fast image acquisition [24] and simultaneous optical particle trapping at a specific position relative to the cell.

Biomedical Optics EXPRESS

3D images were recorded in 2 steps. First, the illumination beam was scanned in x-direction during the integration time of the camera. The focus of the ETL was adjusted to image the illuminated plane onto the camera. Second, the illumination beam was shifted by Δz in horizontal z-direction to illuminate the next sample plane in a vertical distance $\Delta y = \Delta z$, through deflection of the 45° micro mirror (see inset of Fig. 2). Simultaneously, the focal power of the ETL was adjusted to image the next illumination plane. This process was repeated to obtain a 3D image stack. The axial scanning range (y-direction) was limited by the tuning range of the ETL, which limits the height of 3D images to 20 µm. To investigate different imaging modalities, we used line-confocal [25] and wide-field detection for both Gaussian and Bessel beams

2. Materials and methods

Mechanical parts required for precise placement of the mirror were custom designed using CAD software considering the space constraints of the PFM. As shown in Fig. 3(a), the fixed part was designed with 3 v-groves at 120° to each other to enable kinematic mounting. The removable part was assembled from 3 parts to provide various degrees of freedom to adjust the mirror during alignment and calibration. While the first part manufactured from Aluminum with 3 threaded holes aligned with v-groves of the fixed part, the second part was made of brass with v-groves running along the sides. This part glides over 4 screws from the sides, pushed by springs from the back against 2 screws at the front. Finally, the micro fabricated mirror was glued to the end of the third part using polymer based adhesive. This arrangement allows all 6 degrees of freedom to be adjusted, which is useful for precise light-sheet alignment. The design is stable with a mirror placement precision of a few micrometers, when the removable part was taken off for sample or coverslip replacement. However, it should be noted that adjustments are not independent of each other, resulting in some extra calibration time.

Mirrors were fabricated with in-house cleanroom processing using polished Silicon wafer (surface roughness < 50 nm rms). The dimensions of the mirror were constrained by the optical tweezers configuration, which should not be obstructed by light-sheet imaging. During initial experiments, two types of mirrors were designed with a width of 120 µm to enable maximum volume imaging. The type 1 mirror was fabricated with dicing of the Aluminum coated wafer as strips of mirror with width 120 µm as shown in Fig. 3(b). Due to their size, type 1 mirrors were difficult to bond to the mirror holder shown in Fig. 3(a). Therefore, a type 2 mirror with broader mirror base (500 µm) was developed. However, the fabrication involved more steps including (i) oxide and nitride deposition, (ii) photolithography, (iii) reactive ion etching (RIE), (iv) resist stripping, (v) KOH etching, (vi) evaporation and (vii) dicing as shown in Fig. 3(b).

The initial calibration of the setup was performed by imaging free floating fluorescence beads in water. The position of the micro mirror and the tilt of the scan mirror were adjusted to get the sharp image throughout the field of view. After calibration, living cells were placed in the sample chamber. Due to inherent beam spreading, a portion of the sample close to the coverslip was not illuminated. This made it necessary to lift the cells off the coverslip by some 50 µm. Therefore, cells were grown on a drop of matrigel on the coverslip that acted as support structure to lift the sample and enable illumination of entire cells. Images were captured with rolling shutter mode of the sCMOS camera (Hamamatsu Orca flash 4.0 V2) with a slit width of 4 pixels for line confocal detection [25, 26] and 400 pixels for non-confocal detection. 3D image stacks (scanning in y-direction) were recorded with the tunable lens. With the 1.2 NA objective lens and the relay lenses L4 and L5, image stacks up to a depth of 20 µm were recorded. The operation of the microscope was controlled by custom software routines written in Python. The laser with wavelength of 491 nm was used for excitation as it was optimal for imaging macrophages labeled with LifeAct GFP.

Biomedical Optics EXPRESS

While both Gaussian and Bessel beams had a depth of field of around 50 µm, the Bessel beam was narrower with diameter of central maximum of around 1 µm than the Gaussian beam with minimum beam width of 2.5 µm. Fluorescent beads fixed in 1.5% Agarose were used for characterization of the system's PSF.

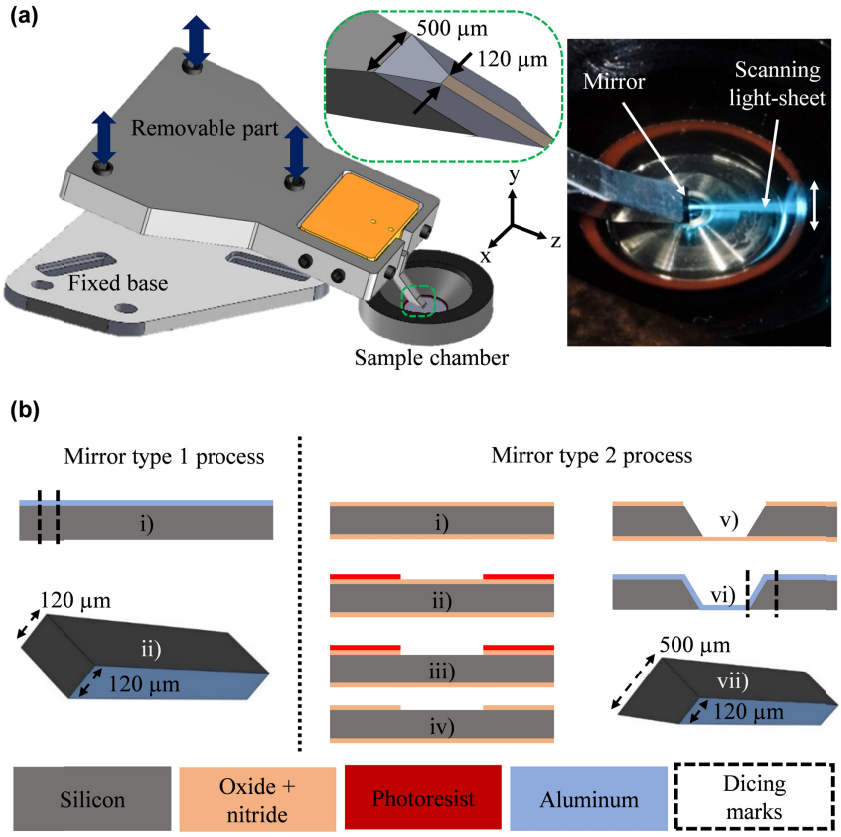

Fig. 3. (a) The mirror holder contains a fixed and a removable part. The fixed base is secured tightly to the microscope and contains v-groves at 120° to each other. The removable part is designed considering the space constraints of the optical tweezer setup and contains various screws for mirror alignment. 3 ball ended screws of the removable part allow to position the micro mirror precisely (precision < 20 µm) after initial adjustments. V-groves ensure a precision placement for a good repeatability and reduced calibration time. (b) 2 types of Silicon mirrors are produced. Type 1 is a silicon wafer (thickness 525 µm) diced in rectangular shape with the width of 120 µm. The aluminum is evaporated on the mirror side for increased reflectance. The mirror is then bonded to the mirror holder using a polymer based adhesive. The type 2 mirror has more steps including photolithography, reactive ion etching (RIE) and KOH (Potassium hydroxide) etching. Due to anisotropic etching of silicon by KOH, type 2 mirror has a bigger base which facilitates the bonding of the mirror to the holder.

3. Results and discussion

3.1 Scanned Gaussian beams

The quality of 3D images regarding contrast and resolution was investigated first by using scanned Gaussian beams, which formed a light-sheet during the integration time of the camera. In a first step, we used 190 nm fluorescent beads embedded in agarose gel on a coverslip and the light-sheet was moved in axial y-direction through the sample in steps of 300 µm. We applied three different imaging modes to investigate the image quality by comparing the signal-to-background ratios (SBR): scanned light-sheet with line-confocal

Biomedical Optics EXPRESS

detection, scanned light-sheet with wide-field detection and wide-field illumination and detection.

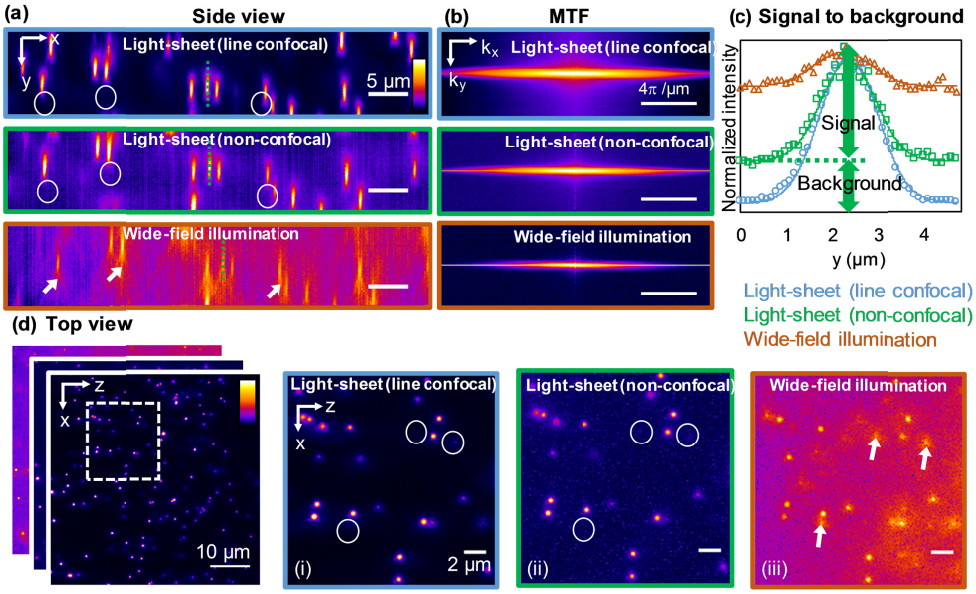

Fig. 4. Comparison of light-sheet illumination with Gaussian beam scanning and widefield epi-fluorescence. (a) Side view of images from 190 nm beads show significant improvement in the image quality for light-sheet illumination. Cirles indicate the reduced background in the light-sheet images compared to the epifluorescent image (see arrows). Improved sectioning can be seen also in the top view (image (d)) where the defocussed beads remain invisible in light-sheet images. (b) The modulation transfer functions (MTF) of the corresponding side view images show a spectrum broadening in axial direction for light-sheet illumination. (c) The normalized linescans from figure (a) also show reduced background for images with light-sheet illumination. (d) light sheet images suppress the out-of-focus beads efficiently (indicated by circles), which remain visible in wide-field illumination (indicated by the arrows).

Figure 4(a) shows three side views of bead images, which appear elongated in detection direction (y) and which reveal different background intensities. The intensity line scans from three exemplary bead images (see dashed lines) along y direction are plotted in Fig. 4(c) and clearly demonstrate the improvement in SBR with light-sheet illumination especially for the line-confocal mode. The analysis revealed a SBR = 17 for the line-confocal mode, a SBR = 3.2 for the non-confocal mode and a SBR = 1.25 for the wide-field mode. Furthermore, the Modulation Transfer Functions MTF(k_x,k_y), approximated by the Fourier transforms of the images p(x,y), are displayed in Fig. 4(b). Here, the increased broadening of the k-spectrum along k_y shows the effect of light-sheet illumination, especially in the line confocal mode. The effects are also visible in top view as shown in Fig. 4(d), where out-of-focus bead images (see arrows in magnified image iii) are efficiently suppressed with light-sheet illumination (see circles in magnified images i and ii). Once more, the line confocal images reveal a better contrast than the non-confocal light-sheet images. However, imaging of living cells is significantly more complicated, since cells move and rearrange, scatter more strongly and usually are labeled with less fluorophores in comparison to most beads.

To demonstrate the performance of our miniature light-sheet, live cells were imaged using scanned Gaussian beams. Figure 5(a) shows 3D sections of GFP-actin (LifeAct-GFP) labeled primary mouse macrophages embedded in Matrigel, which were imaged in line-confocal light-sheet mode. In Fig. 5(b), cross-sections at different heights through a single cell are shown. Due to the good image contrast, small protrusions such as filopodia and lamellipodia at the cell periphery are visible. In a further step, the miniature light-sheet system was used to

Biomedical Optics EXPRESS

image mammalian breast cancer cells in a cluster (Fig. 5(c)). The shape and the nuclei of the propidium iodide stained cells were visible although the sample was highly scattering.

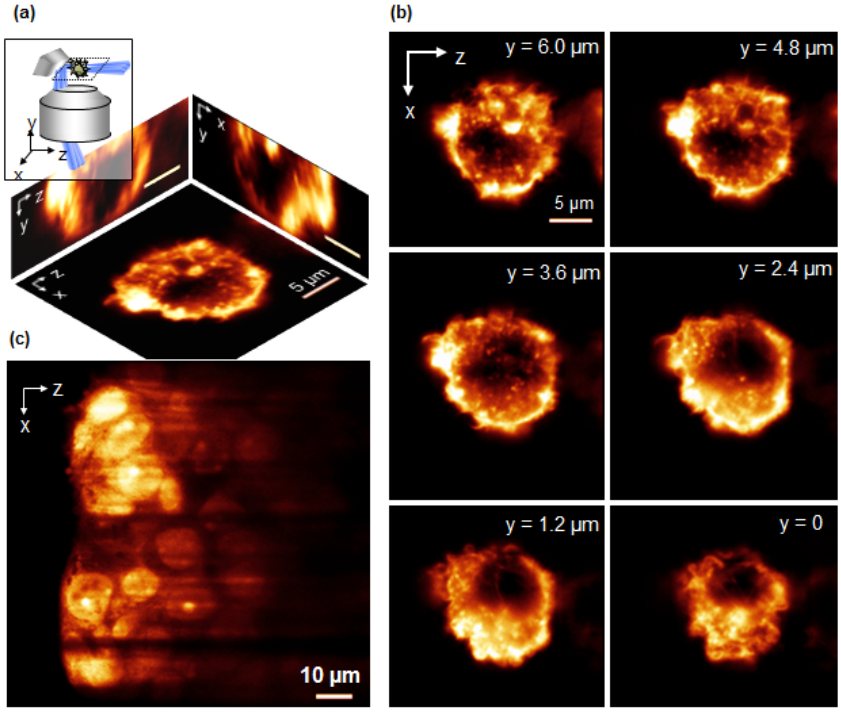

Fig. 5. (a) 3D section of primary macrophages grown on matrigel. (b) Top view images through primary macrophage, separated by 1.2 µm. (c) A section through cell spheroids containing mammalian cancer cells (cell line T47D).

3.2 Scanned Bessel beams

The achromatic lens was replaced by the axicon (see Fig. 2) to enable light-sheet illumination with scanned Bessel beams for further improvement in axial resolution. The line-confocal detection mode implemented in the sCMOS camera and in our self-written software suppresses the background fluorescence generated by the surrounding concentric ring system. The maximum projection of 190 nm beads diffusing through the beam (Fig. 6(a)) displays the surrounding concentric ring system [25, 27], which is characteristic to Bessel beams. The difference between line confocal and non-confocal detection is shown in Fig. 6(b, c) with xy cross-sections of fixed beads imaged with our miniature scanned Bessel beam light-sheet. The axial PSFs fitted with Gaussian function (Fig. 6(d)) clearly indicate the improvement in axial resolution with line confocal-detection.

It can be seen that both the lateral and axial FWHM of the bead images (approximated PSF) hardly spread along the propagation direction of the Bessel beam (Fig. 7(a, b)). In addition, the mean non-confocal FWHM of 1.01 ± 0.08 µm µm was decreased by 23% to a 0.78 ± 0.07 µm mean FWHM in line-confocal mode. This improvement is also validated in the MTFs averaged over 512 slices (Fig. 7(c, d)) and the corresponding line scans in axial and lateral directions.

The lateral widths of the bead images (FWHM = 0.42µm) are always broader than of a PSF alone. Furthermore, a small broadening is caused by spherical aberrations induced by a slight refractive index mismatch of the gel embedding the beads, which were in a distance of 50-100 µm to the coverslip.

Biomedical Optics EXPRESS

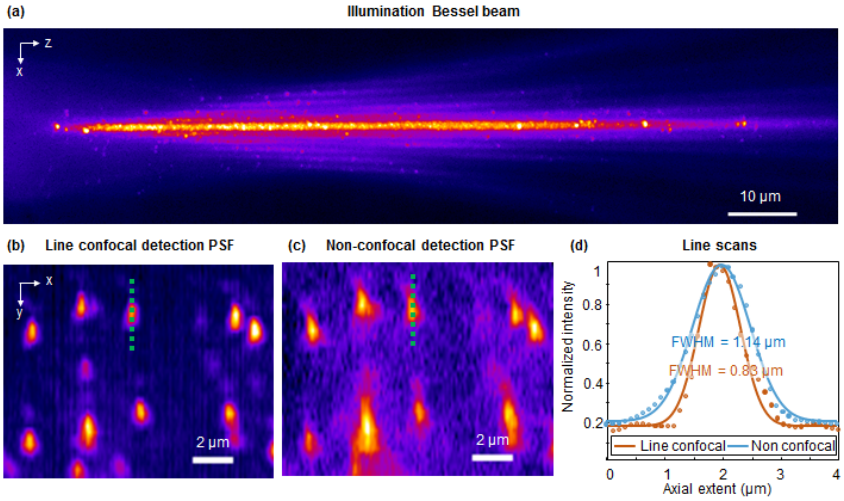

Fig. 6. (a) Maximum projection of images of fluorescent beads (diameter = 190 nm) freely diffusing in water excited by a static Bessel beam. The image shows the thin, long and propagation-stable central maximum and the surrounding ring system of the Bessel beam. (b) and (c) xy-cross-section of the static beads imaged with line-confocal detection and non-confocal detection. (d) Line scans of the beads in (b) and (c) show improvement in axial full-width half-maximum (FWHM) with line confocal detection compared to non-confocal detection.

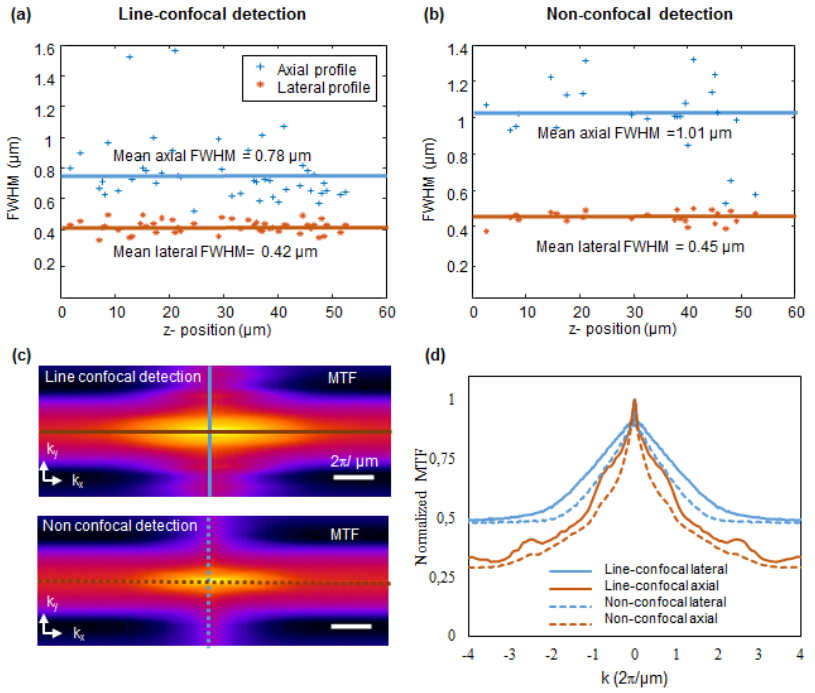

Fig. 7. (a) and (b) Lateral and axial PSF widths (FWHM) along the propagation direction (z) for line-confocal and non-confocal detection. (c) The averaged modulation transfer functions (MTFs) show a frequency spectrum (logarithmic scale), which is broadened in k_y-direction for line-confocal detection compared to non-confocal detection. (d) Horizontal line scans (in brown) and vertical (in blue) line scans through the MTF.

Biomedical Optics EXPRESS

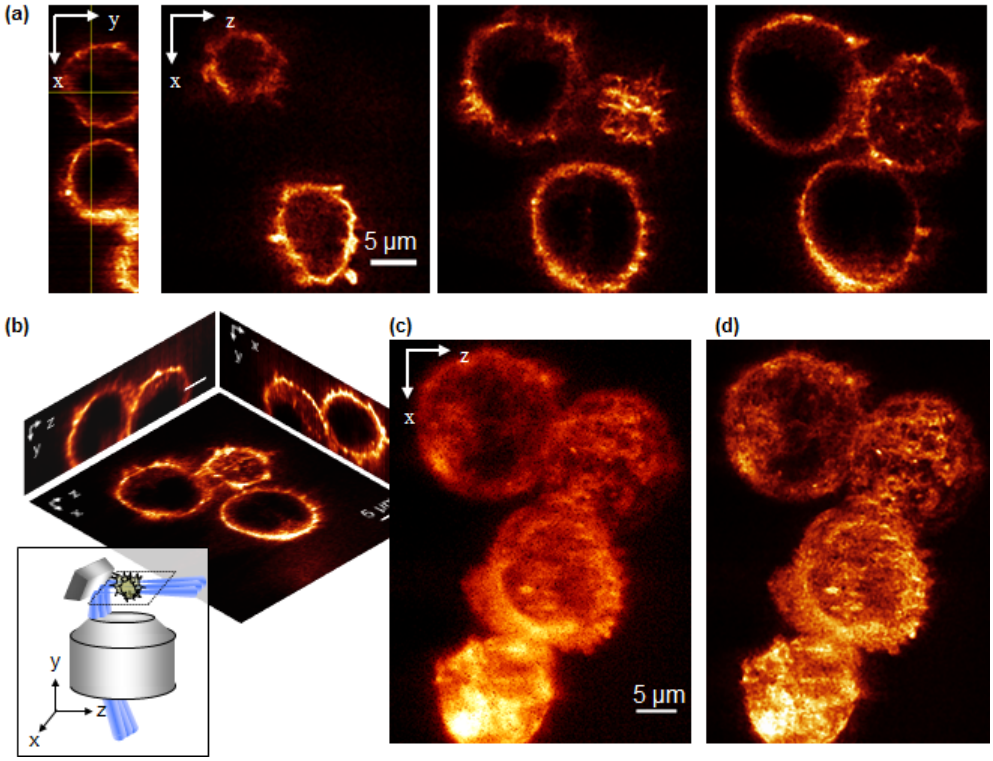

Fig. 8. J774 mouse macrophages grown on Matrigel were illuminated with Bessel beams and imaged in line confocal mode. (a) Side view and top views of deconvolved images at different heights. (b) 3D sections of deconvolved images. (c) Maximum projection of unprocessed images. (d) Maximum projection of deconvolved images.

To demonstrate the live cell imaging capability of our miniature light-sheet system, live J774 mouse macrophages (labelled with LifeAct-GFP) grown on a Matrigel were imaged with Bessel beam illumination and line-confocal detection. The images shown in Fig. 8(a, b) were deconvolved with Microvolution (Microvolution, llc, USA) to demonstrate the near maximal possible quality. The xz-cross-sections at different heights show multiple cellular protrusions with very low background. In Fig. 8(c, d) the deconvolution effect is shown by the maximum projections of unprocessed and deconvolved images. Further comparison of an unprocessed image section from our setup with commercial microscopy techniques such as Epi-fluorescence or Confocal Spinning Disc (Fig. 9) shows the capability of our custom built Mini Bessel light-sheet setup. Our solution clearly outperforms epi-fluorescence, but cannot compete with confocal spinning disc, which is however not applicable in combination with PFM.

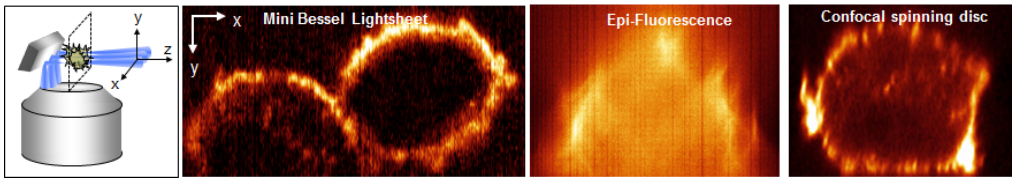

Fig. 9. Comparison of unprocessed xy-cross-sections from 3D images of different J774 mouse macrophages recorded with our miniature Bessel beam light-sheet setup, with conventional Epi-fluorescence and with commercial Confocal Spinning disc microscopy.

Biomedical Optics EXPRESS

A comparable miniature reflected light-sheet microscope (RLSM) [11], used an AFM cantilever and an opposing lens displaced relative to the objective lens. However, this prevents a combination with other optical techniques based on opposing objective lenses with a common optical axis. While Gebhardt et al. [11] introduced RLSM for single molecule tracking with reduced background, 3D imaging was not demonstrated, which is a key application in LSM. Furthermore, we do not need an opposing lens, since our micromirror is mounted kinematically on the stage.

4. Summary and conclusion

In this study we have presented a miniature light-sheet illumination system, which can be combined with an inverted high-NA light microscope and an optical tweezers setup, without the need for any microscope reconstruction. It consists of a cantilevered micro mirror, which is positioned by a standard kinematic mounting with baseplate fixed on the microscope frame.

In our 3D LSM setup, we applied a reflecting area of 0.12 mm × 3 mm is sufficient to scan both Gaussian beams and Bessel beams through the focal plane of a NA = 1.2 water immersion lens using standard galvanometric scan mirrors. The same scan mirrors are used to displace the resulting light-sheet also in axial direction, thus keeping the setup relatively simple. The resulting scan volume was about $\Delta x\Delta y\Delta z \approx 100\ \mu m \times 50\ \mu m \times 60\ \mu m$, the detection volume currently limited to $\Delta y = 20\mu m$ due to the focal range of the electro optical tunable lens (ETL). Living cells can be placed inside or on top of gels of different mechanical/biochemical properties, which were mounted directly on a standard coverslip. Gels should not be too viscous to allow displacement of the cantilevered micro mirror.

Our design motivation was to avoid any displacement of the cell on the coverslip during recordings to enable simultaneous experiments with optical tweezers. Here, a constant and stable trapping focus must hold a trapped particle (or bacteria) at a well-defined position relative to the cell periphery. In our application, the design geometry of the micro mirror was further constrained by a water dipping lens opposing the objective lens at a fixed distance, thus enabling fast 3D particle position tracking. However, another decisive advantage of not displacing the sample in axial direction, but of moving the scanned light-sheet up and down is imaging speed. Although not shown in this study, this allows 2D image acquisition at several hundred Hz [24] by refocusing the fluorescence light emitted inside the light-sheet onto the camera with an ETL. In this way 3D image stacks can be recorded sufficiently fast to investigate the complex dynamics of cells, in particular of cellular protrusions.

We could show that scanned Gaussian and scanned Bessel beams in combination with line-confocal detection achieve a resolution of 0.42 µm laterally and 0.78 µm axially, while providing a more than 10-fold improved image contrast in comparison to conventional fluorescence microscopy. The images of living mouse macrophages, cells that have a rather dense cell cortex, are of high quality and provide excellent sectioning, as demonstrated in this study. Although experiments with optical tweezers have not been performed in this study, mounting living cells on top of the gel and approaching an optically trapped bead to the cell periphery is straightforward. We strongly believe that add-on systems to standard microscopes - similar to our presented system - will have great impact on future 3D life cell imaging applications, especially when speed and reduced fluorophore bleaching are of significant relevance.

Funding

German Research Foundation (DFG); Albert Ludwigs University Freiburg Open Access Publishing Fund.

Acknowledgment

We thank Dr. Tim Lämmermann for providing primary mouse macrophages and matrigel for experiments, Dr. Andreas Thomsen for providing cell clusters, Birgit Erhard for help with cell

Biomedical Optics EXPRESS

culture and preparation, and the BIOSS toolbox from the BIOSS Center of Excellence (University of Freiburg) for transfection of J774 macrophages. We also thank Dr. Mika Ruonala for the deconvolution and Dr. Felix Juenger for helpful comments on the manuscript.

The article processing charge was funded by the German Research Foundation (DFG) and the Albert Ludwigs University Freiburg in the funding programme Open Access Publishing.

Disclosures

The authors declare that there are no conflicts of interest related to this article.

References

1. F. Jünger, P. V. Olshausen, and A. Rohrbach, "Fast, label-free super-resolution live-cell imaging using rotating coherent scattering (ROCS) microscopy," Sci. Rep. **6**(1), 30393 (2016).
2. S. Diez, G. Gerisch, K. Anderson, A. Müller-Taubenberger, and T. Bretschneider, "Subsecond reorganization of the actin network in cell motility and chemotaxis," Proc. Natl. Acad. Sci. U.S.A. **102**(21), 7601–7606 (2005).
3. J. Huisken, J. Swoger, F. Del Bene, J. Wittbrodt, and E. H. K. Stelzer, "Optical sectioning deep inside live embryos by selective plane illumination microscopy," Science **305**(5686), 1007–1009 (2004).
4. O. E. Olarte, J. Andilla, E. J. Gualda, and P. Loza-Alvarez, "Light-sheet microscopy: a tutorial," Adv. Opt. Photonics **10**(1), 111–179 (2018).
5. E. G. Reynaud, U. Kržič, K. Greger, and E. H. K. Stelzer, "Light sheet-based fluorescence microscopy: more dimensions, more photons, and less photodamage," HFSP J. **2**(5), 266–275 (2008).
6. B. C. Chen, W. R. Legant, K. Wang, L. Shao, D. E. Milkie, M. W. Davidson, C. Janetopoulos, X. S. Wu, J. A. Hammer 3rd, Z. Liu, B. P. English, Y. Mimori-Kiyosue, D. P. Romero, A. T. Ritter, J. Lippincott-Schwartz, L. Fritz-Laylin, R. D. Mullins, D. M. Mitchell, J. N. Bembenek, A. C. Reymann, R. Böhme, S. W. Grill, J. T. Wang, G. Seydoux, U. S. Tulu, D. P. Kiehart, and E. Betzig, "Lattice light-sheet microscopy: imaging molecules to embryos at high spatiotemporal resolution," Science **346**(6208), 1257998 (2014).
7. P. J. Keller, A. D. Schmidt, J. Wittbrodt, and E. H. K. Stelzer, "Reconstruction of zebrafish early embryonic development by scanned light sheet microscopy," Science **322**(5904), 1065–1069 (2008).
8. F. O. Fahrbach, P. Simon, and A. Rohrbach, "Microscopy with self-reconstructing beams," Nat. Photonics **4**(11), 780–785 (2010).
9. M. Tokunaga, N. Imamoto, and K. Sakata-Sogawa, "Highly inclined thin illumination enables clear single-molecule imaging in cells," Nat. Methods **5**(2), 159–161 (2008).
10. Y. Wu, A. Ghitani, R. Christensen, A. Santella, Z. Du, G. Rondeau, Z. Bao, D. Colón-Ramos, and H. Shroff, "Inverted selective plane illumination microscopy (iSPIM) enables coupled cell identity lineaging and neurodevelopmental imaging in Caenorhabditis elegans," Proc. Natl. Acad. Sci. U.S.A. **108**(43), 17708–17713 (2011).
11. J. C. M. Gebhardt, D. M. Suter, R. Roy, Z. W. Zhao, A. R. Chapman, S. Basu, T. Maniatis, and X. S. Xie, "Single-molecule imaging of transcription factor binding to DNA in live mammalian cells," Nat. Methods **10**(5), 421–426 (2013).
12. Y. S. Hu, Q. Zhu, K. Elkins, K. Tse, Y. Li, J. A. J. Fitzpatrick, I. M. Verma, and H. Cang, "Light-sheet Bayesian microscopy enables deep-cell super-resolution imaging of heterochromatin in live human embryonic stem cells," Opt. Nanoscopy **2**(1), 7 (2013).
13. R. Galland, G. Grenci, A. Aravind, V. Viasnoff, V. Studer, and J. B. Sibarita, "3D high- and super-resolution imaging using single-objective SPIM," Nat. Methods **12**(7), 641–644 (2015).
14. M. B. Bouchard, V. Voleti, C. S. Mendes, C. Lacefield, W. B. Grueber, R. S. Mann, R. M. Bruno, and E. M. C. Hillman, "Swept confocally-aligned planar excitation (SCAPE) microscopy for high speed volumetric imaging of behaving organisms," Nat. Photonics **9**(2), 113–119 (2015).
15. C. Dunsby, "Optically sectioned imaging by oblique plane microscopy," Opt. Express **16**(25), 20306–20316 (2008).
16. T. Bruns, M. Bauer, S. Bruns, H. Meyer, D. Kubin, and H. Schneckenburger, "Miniaturized modules for light sheet microscopy with low chromatic aberration," J. Microsc. **264**(3), 261–267 (2016).
17. Z. Yang, P. Piksarv, D. E. K. Ferrier, F. J. Gunn-Moore, and K. Dholakia, "Macro-optical trapping for sample confinement in light sheet microscopy," Biomed. Opt. Express **6**(8), 2778–2785 (2015).
18. K. Bambardekar, R. Clément, O. Blanc, C. Chardès, and P. F. Lenne, "Direct laser manipulation reveals the mechanics of cell contacts in vivo," Proc. Natl. Acad. Sci. U.S.A. **112**(5), 1416–1421 (2015).
19. F. Jünger, F. Kohler, A. Meinel, T. Meyer, R. Nitschke, B. Erhard, and A. Rohrbach, "Measuring local viscosities near membranes of living cells with photonic force microscopy," Biophys. J. **109**(5), 869–882 (2015).
20. H. Kress, E. H. K. Stelzer, D. Holzer, F. Buss, G. Griffiths, and A. Rohrbach, "Filopodia act as phagocytic tentacles and pull with discrete steps and a load-dependent velocity," Proc. Natl. Acad. Sci. U.S.A. **104**(28), 11633–11638 (2007).
21. F. Kohler and A. Rohrbach, "Surfing along filopodia - a particle transport revealed by molecular scale fluctuation analyses," Biophys. J. **108**(9), 2114–2125 (2015).

Biomedical Optics EXPRESS

22. M. Griesshammer and A. Rohrbach, "5D-Tracking of a nanorod in a focused laser beam--a theoretical concept," Opt. Express **22**(5), 6114–6132 (2014).
23. H. Kress, E. H. K. Stelzer, G. Griffiths, and A. Rohrbach, "Control of relative radiation pressure in optical traps: application to phagocytic membrane binding studies," Phys. Rev. E Stat. Nonlin. Soft Matter Phys. **71**(6), 061927 (2005).
24. F. O. Fahrbach, F. F. Voigt, B. Schmid, F. Helmchen, and J. Huisken, "Rapid 3D light-sheet microscopy with a tunable lens," Opt. Express **21**(18), 21010–21026 (2013).
25. F. O. Fahrbach and A. Rohrbach, "Propagation stability of self-reconstructing Bessel beams enables contrast-enhanced imaging in thick media," Nat. Commun. **3**(1), 632 (2012).
26. E. Baumgart and U. Kubitscheck, "Scanned light sheet microscopy with confocal slit detection," Opt. Express **20**(19), 21805–21814 (2012).
27. T. Meinert, O. Tietz, K. J. Palme, and A. Rohrbach, "Separation of ballistic and diffusive fluorescence photons in confocal Light-Sheet Microscopy of Arabidopsis roots," Sci. Rep. **6**(1), 30378 (2016).